metals

MDPI

Article

Effect of Rolling Reduction on Microstructures and Mechanical Properties of Sc-Containing Al-3.2Cu-1.5Li Alloy

Jian Wang [1,2], Yun Kan [1], Wenting Xu [1], Yalin Lu [1,*], Dongshuai Zhou [1] and Shenao Li [1]

[1] School of Materials Engineering, Jiangsu University of Technology, Changzhou 213001, China; wjhjj1217@163.com (J.W.)
[2] College of Mechanical and Electrical Engineering, Hohai University, Changzhou 213022, China
* Correspondence: luyalin@163.com

Abstract: The effects of various rolling reductions (64.7%, 72.1%, 81.4% and 88.2%) on the microstructures and mechanical behaviors of Sc-containing Al-3.2Cu-1.5Li-based alloys were experimentally investigated through XRD, SEM (equipped with EBSD), TEM and the tensile test. The results showed that the grains of hot-rolled and T6-treated alloys are mainly dominated by substructure features, and the addition of the trace Sc element can obviously impede the static and dynamic recrystallization due to the formation of fine and stable nano-Al_3(Sc, Zr) particles. Additionally, the combined effects of fine grains, dispersion, substructure and precipitation strengthening make the alloys with a rolling reduction of 81.4% possess higher tensile properties. With an increase in the rolling reduction, the tensile strength of the alloys increases first and then decreases, while the elongation gradually increases and then reaches a plateau, which was ascribed to the variation in the grain size and substructure features.

Keywords: Al-3.2Cu-1.5Li alloy; minor Sc; microstructures; mechanical properties

Citation: Wang, J.; Kan, Y.; Xu, W.; Lu, Y.; Zhou, D.; Li, S. Effect of Rolling Reduction on Microstructures and Mechanical Properties of Sc-Containing Al-3.2Cu-1.5Li Alloy. *Metals* **2023**, *13*, 770. https://doi.org/10.3390/met13040770

Academic Editor: Frank Czerwinski

Received: 2 March 2023
Revised: 2 April 2023
Accepted: 7 April 2023
Published: 14 April 2023

1. Introduction

Al-Cu-Li alloys have attained extensive attention because of their superior performances involving high specific strength and excellent resistance to damage [1]. Therefore, it is urgent to prepare advanced Al-Cu-Li alloys utilized for various engineering demands by regulating the size, distribution and number density of the major strengthening phases. A practical approach for improving the microstructures and mechanical behaviors of Al-Cu-Li alloys usually focuses on the addition of microalloying elements and plastic deformation technology. It is well accepted that microalloying, severe plasticity deformation and heat treatment can modify the precipitation action of submicron/nanoscale hardening phases, thus adjusting the mechanical behaviors of Al-Cu-Li alloys [2–4]. For instance, introducing minor microalloying elements (such as Zn, Mg and Ag) into Al-Cu-Li alloys can notably accelerate the formation of the T_1 phase, which is typically considered to produce a vital effect in strengthening the alloy system [4–6]. However, as a microalloyed element with the characteristics of transition elements and rare earth elements, the mechanisms of the Sc element on Al-Cu-Li alloys are still controversial.

Severe plasticity deformations (SPDs) are commonly used to obtain high-density available defects in the microstructure and refine the grain size, thus achieving the enhancement of mechanical behaviors [7–12]. Fan et al. [9] investigated the effects of various rolling processes on the precipitation behaviors and consequent tensile properties of the AA2195 alloy, and they attributed the excellent combination of strength and ductility to the strong intensity of the brass texture and high number density of the T_1 phases. Various prior heat treatments have been implemented before hot rolling by Yang et al. [10], and the authors mentioned that the extensive planar slips markedly affect the evolution of the hot rolling texture. The hot-rolled alloy at 280 °C exhibited the highest tensile strength in

a longitudinal direction due to the enhanced volume fraction of the rolling textures and higher number density of the T_1 phases [11]. Moreover, Medjahed et al. [12] stated that the alloy with a 90° rolling orientation exhibited the desirable mechanical properties, which were closely correlated with the uniformly dispersed strengthening precipitates along the various tensile angles.

The effects of Sc addition on the mechanical behaviors of Al-Cu-Li alloys with different Cu/Li ratios are double-edged. According to the Al-Cu-Sc phase diagram, a thermally stable W phase (AlCuSc) was formed, which is highly dependent on the Cu content and the minor Sc addition in Al-Cu-Li alloys [13]. When Sc is introduced into Al-Cu-Li alloys with a low content of Cu or without Cu, the Sc atoms tend to combine with Al atoms to form $A1_3Sc$ particles wrapped by δ′ (Al_3Li) particles and exist as Al_3(Sc, Zr) composite particles [14]. For some Al-Cu-Li alloys with higher Cu/Li ratios (Cu/Li > 2.8), such as 1469 [15,16], 2070 [17] and the new Al-3.8Cu-1.2Li alloy [18], the addition of minor Sc exerts some negative function on the strength. However, the improved hardness and strength are presented in the AA2195 alloy (Cu/Li = 3.3) with the addition of Sc, and the authors attributed this phenomenon to the refined grain and fine dispersed Al_3(Sc, Zr) particles [19]. Conversely, when adding a minor Sc element to some Al-Cu-Li alloys with lower Cu/Li ratios (Cu/Li < 1.8), such as the 2099 [20], 1445 [21] and 1460 alloys [22], enhanced strength was attained, although W phases were possibly formed, which was correlated to the existence of nanoscale Al_3(Sc, Zr) particles. However, as the Sc content was further increased to 0.22%, the strength of the 1460 alloy was then decreased. A reasonable explanation for this phenomenon may be related to the fact that the enhanced strength caused by the Al_3(Sc, Zr) particles cannot compensate for the strength loss decided by the reduction in the T_1 phase content due to the formation of more Cu-rich and Sc-contained W phases.

Based on the above literature analyses, existing research efforts have mainly concentrated on the evolution of the microstructure and properties of the Sc-containing Al-Cu-Li alloys with a higher or lower Cu/Li ratio. Therefore, in this work, trace Sc was added to the Al-Cu-Li alloy with a medium Cu/Li ratio (Cu/Li ≈ 2.1), and the corresponding microstructures and mechanical properties were investigated to clarify that the rolling deformation induces microstructures and property changes and the microalloying effect of Sc in this kind of Al-Cu-Li alloy.

2. Materials and Experiments

The studied alloys were prepared by a vacuum medium frequency induction furnace (BYT Co., Ltd., Nanjing, China) with raw materials of Al-50Cu, Al-15Mn, Al-10Zr and Al-2Sc master alloys, as well as high-pure Li, pure Mg and pure Zn. The main melting processes are as follows: (I) cutting and polishing the raw materials that need to be used and then cleaning them with acetone; (II) putting the raw materials and square metal mold into the oven (BYT Co., Ltd., Nanjing, China) and preheating them for more than 2 h at 300 °C and then mixing the raw materials into a high-density graphite crucible; (III) heating, melting and electromagnetic stirring of the raw materials under an argon protection atmosphere to improve the uniformity of the melt, adding high-pure Li into the melt with the additional device; and (IV) melting, standing and pouring the fully mixed liquid alloy into the preheated square metal mold. The nominal chemical composition of the alloy is Al-3.2Cu-1.5Li-0.4Mg-0.3Mn-0.3Zn-0.11Zr-0.1Sc (wt. %). After the oxide scale and visible defects of the ingot surface were scalped by mechanical processing, the ingots were two-stage homogenized (470 °C × 10 h + 520 °C × 24 h) in the KF1100 high-temperature box resistance furnace (temperature error ± 2 °C) (BYT Co., Ltd., Nanjing, China) and then air cooled to room temperature.

The homogenized samples with a thickness of 20 mm were hot rolled into plates of 7.06 mm, 5.80 mm, 3.72 mm and 2.36 mm thickness at 420 °C (corresponding to rolling reductions of 64.7%, 72.1%, 81.4% and 88.2%, respectively). Then, the same T6 heat treatment of 510 °C × 1.5 h (quenching in room-temperature water) + 175 °C × 32 h was adopted

simultaneously. After that, the tensile specimens were cut along the rolling direction of the plates with wire-cut electrical discharge machining (WEDM, BMG Co., Ltd., Suzhou, China). The gauge dimension (length × width × thickness) of the tensile specimens was 8 mm × 3 mm × 2 mm. The room-temperature tensile tests were carried out on the specimens with different rolling reductions on a BTM 205D electric universal testing machine (WANCE Co., Ltd., Shenzhen, China) at a strain rate of 2 mm/min. The tensile properties of various process states were determined by tensile tests that were repeated three times, and the mean strength and elongation were then calculated. The detailed sampling positions and dimensions of the tensile specimens are shown in Figure 1.

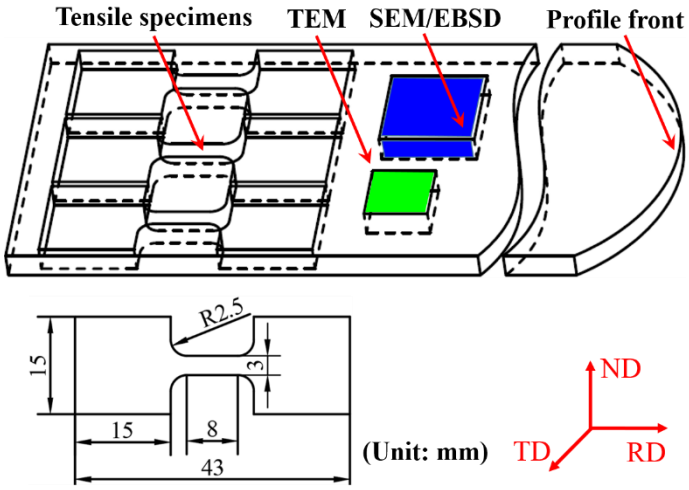

Figure 1. The sampling position and dimensions of tensile specimens.

The samples for microstructure observation were ground with 240#~2000# metallographic sandpaper, mechanically polished and etched with Keller reagent (2 mL HF: 3 mL HCl: 5 mL HNO_3: 190 mL H_2O, volume ratio). The microstructures were observed by a ZEISS Sigma 500 field emission scanning electron microscope (FESEM, Carl Zeiss, Oberkochen, Germany). The grain orientation, recrystallization and misorientation angle distribution of the hot rolled and T6 treated specimens were extracted by electron backscatter diffraction (EBSD, Oxford, London, England), which was attached to the SEM. Electro-polishing was performed at about 2 °C using a standard A2 electrolyte on the Struers Lectropol-5 machine (Struers, Copenhagen, Denmark). A scanning area of 300 × 300 μm^2 and a step size of 0.20 μm were selected for the hot rolled and T6 treated samples. After that, the EBSD data analysis and post-processing were conducted with HKL-Channel 5 software (AZtec 2.0, Oxford, London, England). The melting temperature of eutectic phases of the as-cast and homogenized samples was ascertained by a NETZSCH 404F3 differential scanning calorimeter (DSC, NETZSCH, Selb, Germany) at a constant heating rate of 10 °C/min from room temperature to 700 °C. Phase structure analysis was conducted using a D8 Advance Eco X-ray diffractometer (XRD, Bruker, Karlsruhe, Germany). The TEM observation sample was mechanically thinned to about 60 um by metallographic sandpaper, punched into a small disc with a diameter of 3 mm and then electro-polished using a double-jet electrolytic thinning instrument. After that, the substructure evolution and distribution of the precipitates were characterized by a TALOS F200x TEM (FEI, Boston, MA, USA).

3. Results

Figure 2 presents the microstructural characteristics of the Al-3.2Cu-1.5Li alloy. As shown in Figure 2a, due to the microalloying features of the alloy and the industrial casting process, the as-cast structure of the alloy presents obvious dendritic segregation, and there are a large number of irregular non-equilibrium eutectic phases on the grain boundaries and dendrite arms [17]. For a strain-hardened aluminum alloy, the microstructures of

the ingot could not only directly affect the deformation properties of the alloy but also have pronounced effects on the following working procedures and the final product performance, thus seriously limiting its use [23]. Homogenization treatment can effectively dissolve the non-equilibrium phase, improve dendritic segregation and promote a more uniform distribution of the elements in the matrix. As shown in Figure 2b, after two-stage homogenization treatment (470 °C × 10 h + 520 °C × 24 h), the dendritic-network structures were noticeably eliminated, only a small amount of the second phases appeared in the form of small sphere or strip and the grain boundary width was refined and clearly visible. The first endothermic peak of about 526 °C in the corresponding DSC curve almost completely disappeared (Figure 2c), which also verifies the excellent effect of the homogenization treatment.

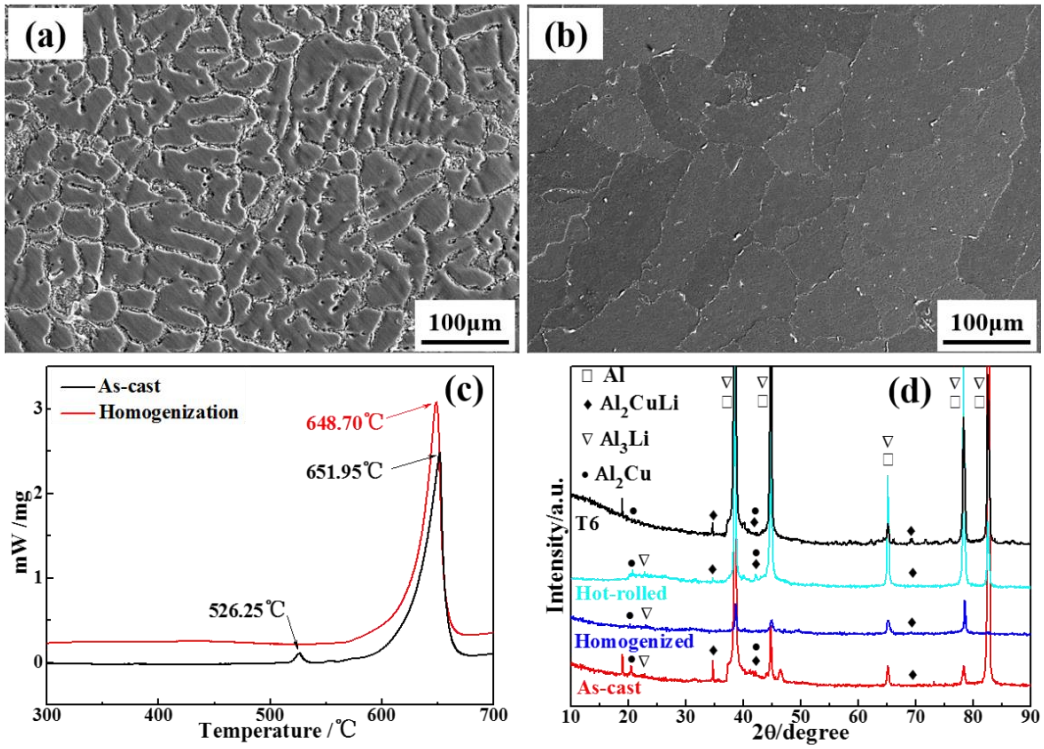

Figure 2. Microstructure characteristics and XRD results of Al-3.2Cu-1.5Li-0.1Sc alloy: (**a**) As-cast microstructure; (**b**) Homogenized microstructure; (**c**) DSC curve of as-cast and homogenized alloy; (**d**) XRD results of alloy in different states.

The grain orientation map, recrystallization map and corresponding misorientation angle distribution (MAD) map obtained by EBSD of the alloys subjected to hot rolling are provided in Figure 3. The misorientation angle between contiguous grains $\theta \geq 15°$ refers to high-angle grain boundaries (HAGBs), as indicated by the black lines, while $3° < \theta < 15°$ stands for low-angle grain boundaries (LAGBs), as marked by the white lines. The different types of grains with a blue color, yellow color and red color denote recrystallized grains, subgrains and deformed grains, respectively. It is clearly observed from Figure 3 that the grains show deformed features with fiber-like grain structures, and there are plenty of flat grains elongated along the rolling direction, with varied grain sizes and shapes. In addition, the grains are smaller in size with an increase in the rolling reduction, implying that increased rolling reduction ensures the grains are more broken and form severe serration with a subgrain scale at the grain boundaries. Similar results were reported by Dong et al. [24]. As can be seen from the MAD map, the misorientation angles of most of the grains are less than 15°, and the accumulative fraction of the boundaries with misorientation angles < 15° is 88%, suggesting that very limited recrystallization occurred in the hot rolled Sc-containing Al-Cu-Li alloys with various rolling reductions. Accordingly,

it was concluded that regardless of the rolling reduction, the formation of recrystallized grains was effectively inhibited.

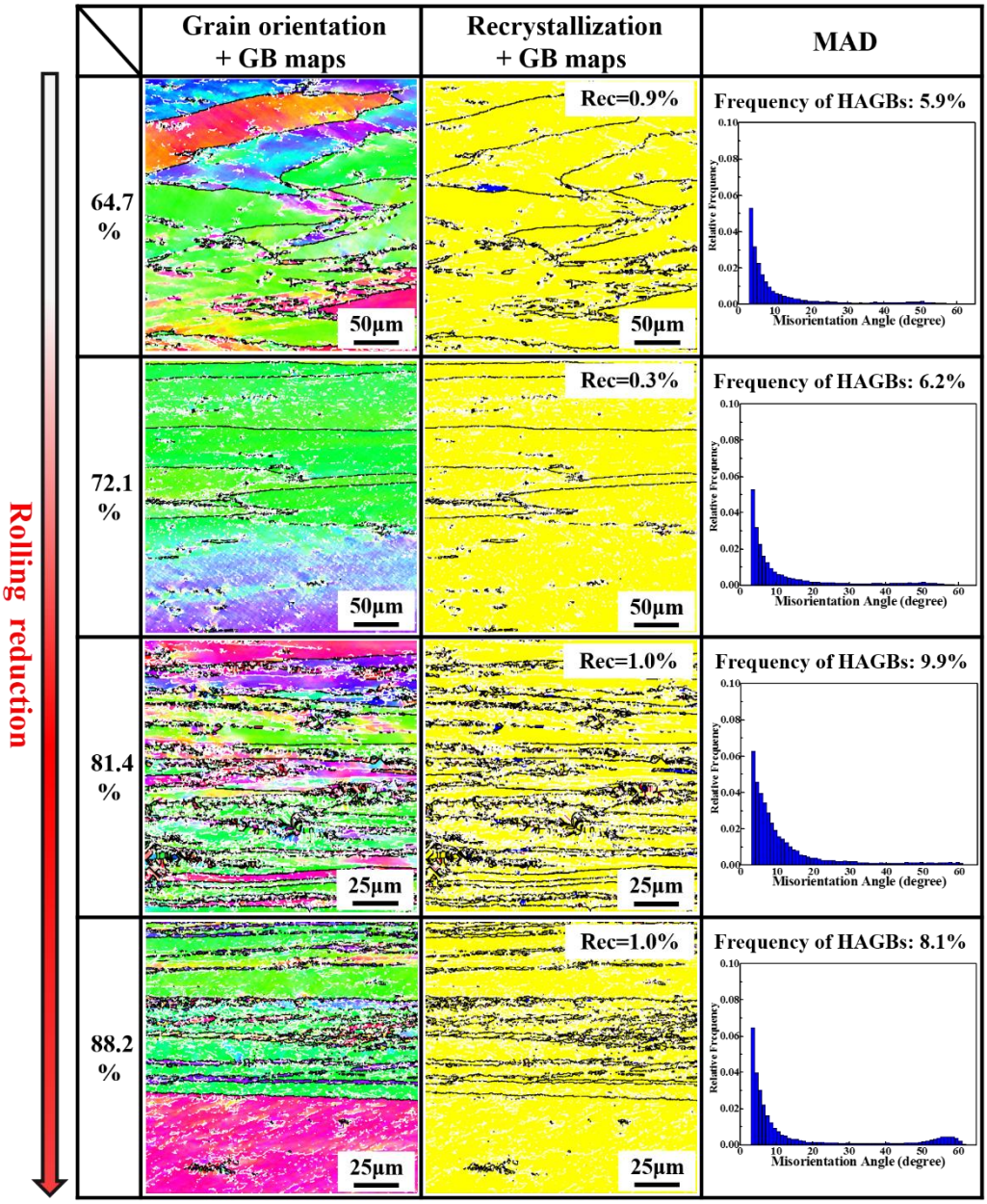

Figure 3. EBSD images of grain structure for the samples with different rolling reductions.

To further investigate the microstructure evolution of the T6-treated Sc-containing alloys, EBSD analysis was performed, as shown by the inverse pole figure (IPF) superimposed with HAGBs and LAGBs, the extent of the recrystallization and the MAD map in Figure 4. After the T6 heat treatment, the microstructural features still exhibit deformed grain structures, and all the alloys comprise larger elongated grains as well as a small amount of fine equiaxed grains. With an increase in the rolling reduction, the recrystallization volume fraction displays a rising trend on the whole, with values of 2.7%, 1.2%, 9.5% and 11.0%, respectively. The changing trend in the radial grain size (RGS) of the T6-treated alloys is consistent with that of the hot rolled state and decreases gradually as the rolling reduction increases. In addition, it is clear that the alloys still present a higher accumulative fraction of boundaries with misorientation angles < 15°. Based on the above, it is reasonable to believe that the addition of minor Sc can produce a grain refinement effect

on the microstructures of the hot-rolled or T6-treated alloys. Meanwhile, the nano-sized Al_3(Sc, Zr) particles precipitated during the homogenization process remarkably inhibit recrystallization and impede the growth of recrystallized grains during hot rolling and T6 heat treatment [18,21].

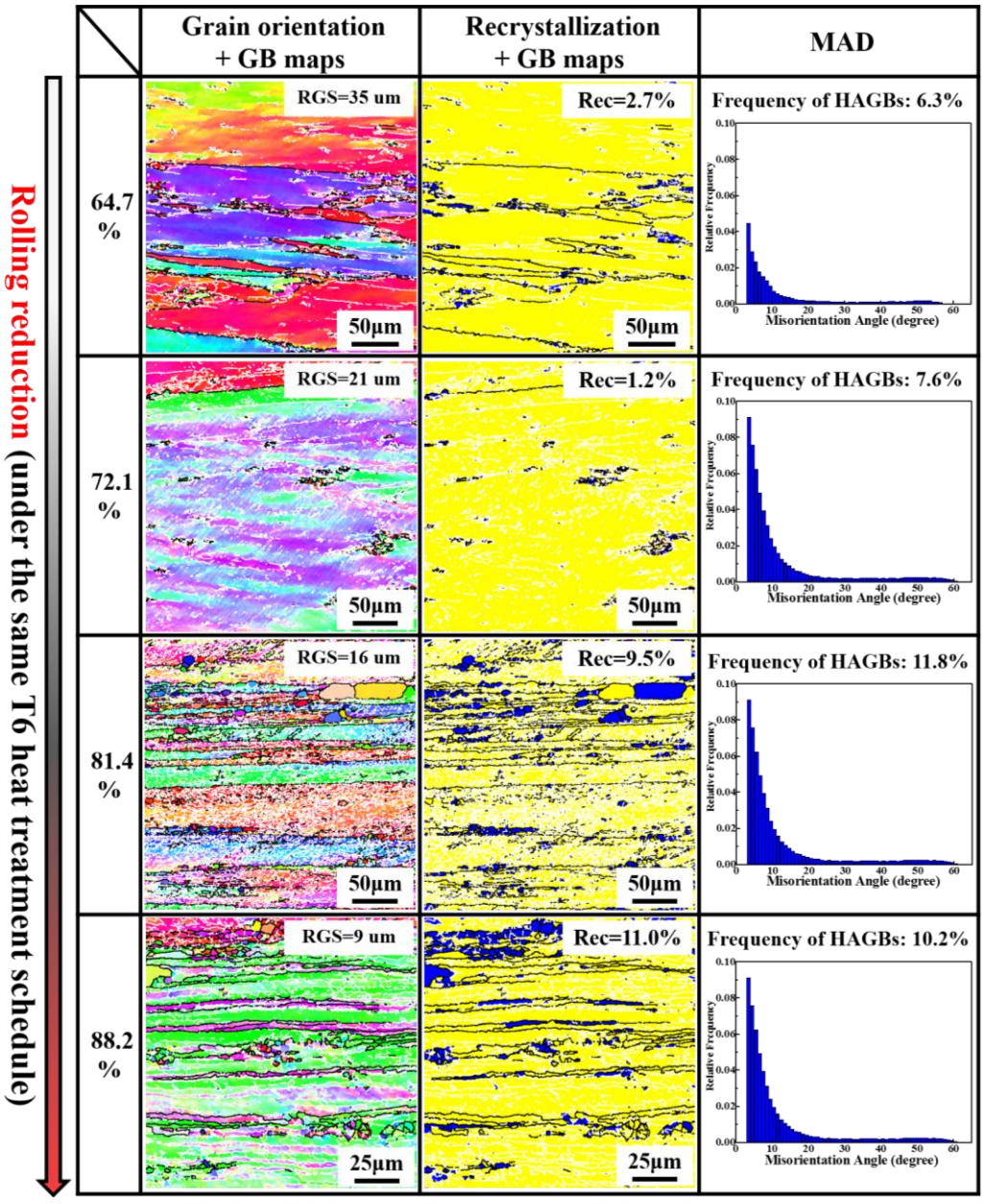

Figure 4. EBSD results of grain structure for the four T6 treated samples after different hot deformation.

Figure 5 displays the TEM microstructures of the Al-3.2Cu-1.5Li-0.1Sc alloy in different states when the rolling reduction is 81.4%. As can be seen from Figure 5a, there are a substantial number of dislocation tangles and dislocation cells in the hot-rolled alloy, and numerous spherical phases are evenly dispersed in the (sub-) grains and (sub-) grain boundaries. Meanwhile, the phenomenon of some spherical phases pinning the dislocations is also observed (Figure 5b). After T6 peak-aging heat treatment, the alloy presents substructure features with the same orientation, a fine (sub-) grain size and a small amount of dislocation cell structures (Figure 5c). Figure 5d–g shows selected area electron diffraction (SAED) patterns captured from the $<112>_{Al}$ and $<100>_{Al}$ zone axes and the

corresponding dark field (DF) TEM images of the studied alloy after T6 treatment followed by hot rolling. As depicted in Figure 5d,e, copious quantities of T_1 phases are precipitated in the alloy matrix, corresponding to the diffraction spots and streaks in the $<112>_{Al}$ SAED pattern. Besides the T_1 phases, the faint streaks along the $<112>_{Al}$ direction arising from the formation of S′ phases are illustrated in Figure 5e. Additionally, the streaks of the θ′ phases are displayed in the $<100>_{Al}$ SAED pattern (Figure 5f), and some θ′ phases are observed in the DF TEM image, as displayed in Figure 5g. Meanwhile, many Al_3Li/Al_3(Sc, Zr) particles are detected (Figure 5g), which already existed in the as-cast and homogenized condition (Figure 2d). Combined with Figure 2d, it can be inferred that the precipitates of the Al-3.2Cu-1.5Li-0.1Sc alloy are mainly numerous T_1 phases, orthogonal θ′ phases and fine dispersed δ′/β′ phases.

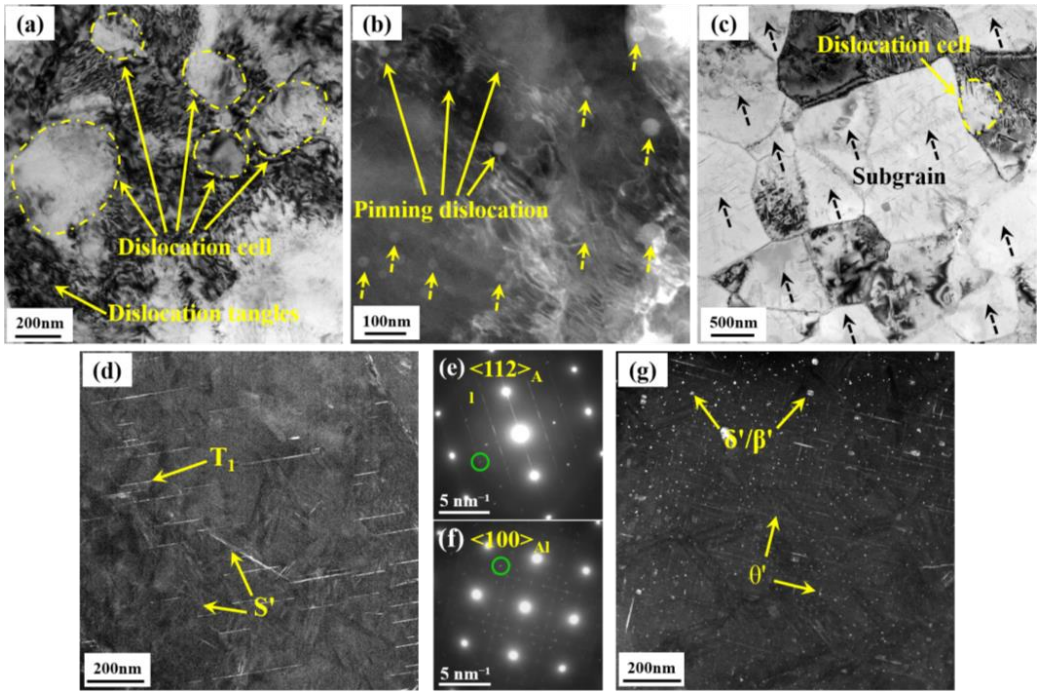

Figure 5. TEM images of alloy with rolling reduction of 81.4% in different states: (**a**) Dislocation morphology of hot-rolled sample; (**b**) HAADF STEM image of spherical particles of hot-rolled sample; (**c**) Substructure of T6 treated sample; (**d**) DF TEM image of T6 treated sample captured from $<112>_{Al}$ zone axis and corresponding SAED pattern of (**e**); (**f**) SAED pattern of T6 treated sample captured from $<100>_{Al}$ zone axis and corresponding DF TEM image of (**g**).

The stress-strain curves of the T6 state Al-3.2Cu-1.5Li-0.1Sc alloys subjected to different amounts of deformation are displayed in Figure 6. It can be seen from Figure 6 that with an increase in the rolling reduction, the tensile strength of the alloys gradually increases and then decreases to the original state. The tensile strengths of the alloys that were hot rolled with deformation of 64.7% and 88.2% exhibit little difference. The tensile strengths of 468.1 ± 5.8 MPa, 471.3 ± 4.3 MPa, 480.4 ± 5.2 MPa and 459.6 ± 6.4 MPa can be achieved at deformations of 64.7%, 72.1%, 81.4% and 88.2%, respectively. Meanwhile, the elongation of the alloys gradually increases and then remains basically unvaried with an increase in the rolling reduction. In addition, the elongation of the alloy reaches 13.0% when the total deformation is 81.4%, which is roughly the same as that obtained at a deformation of 88.2% (12.97%).

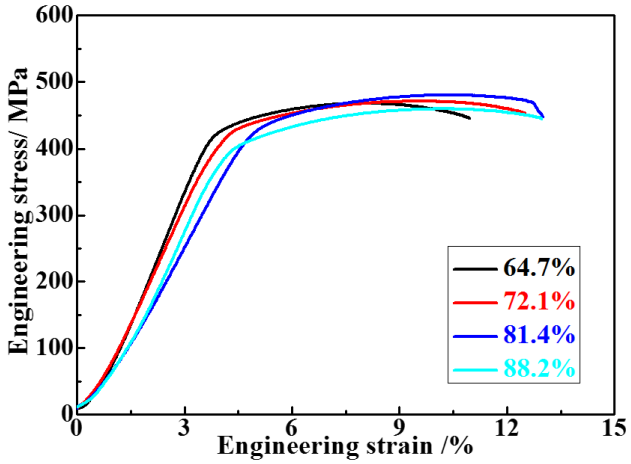

Figure 6. Tensile properties of the T6 treated samples with various rolling reductions.

Figure 7 displays the fractographs of the T6-treated alloys with different rolling reductions. According to Figure 7, all the T6 treated samples exhibit a typical mixed fracture mode of dimple-induced trans-granular fracture and intergranular fracture. As shown in Figure 7a, a small number of shallow dimples, some cleavage surfaces and tear ridges are clearly observed on the fracture surface for the alloy with a rolling reduction of 64.7%. Moreover, for the alloys with higher amounts of rolling reduction, more dimples appeared on the fracture surface, as illustrated in Figure 7b–d, which suggests that the fracture mode was occupied by trans-granular fracture. The reduced fraction of the cleavage surface and the larger range and depth of the dimples presented indicate that the ductility of the Sc-containing alloys is enhanced, which is somewhat associated with the observed tensile test results (Figure 6).

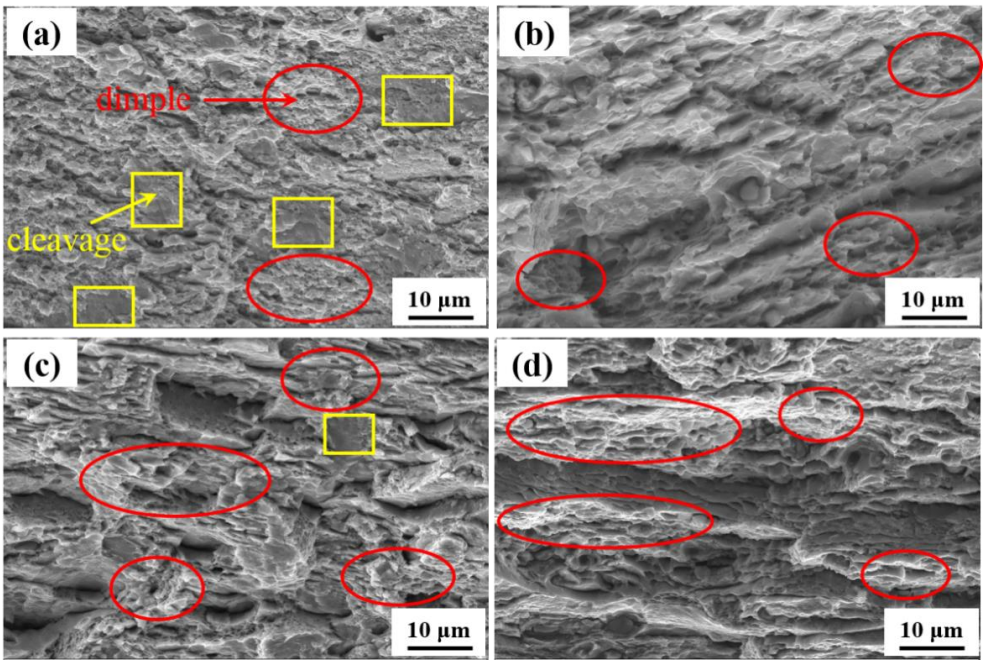

Figure 7. Fracture morphology of the T6 treated alloys with various rolling reductions: (**a**) 64.7%; (**b**) 72.1%; (**c**) 81.4%; (**d**) 88.2%.

4. Discussion

The EBSD results presented in Figures 3 and 4 demonstrate that the recrystallization volume fraction of the hot-rolled Sc-containing alloys is extremely low and remains nearly unvaried, while the volume fraction of the recrystallization shows an overall trend of slight

enhancement after the T6 heat treatment with an increase in the rolling reduction, which is associated with the existence of Al_3(Sc, Zr) particles. A certain amount of primary nano Al_3(Sc, Zr) particles were formed during the solidification process of the Sc-containing Al-Cu-Li alloy [25,26]. These particles can provide heterogeneous nucleation sites to refine the grain structure of as-cast alloys [22]. Al_3(Sc, Zr) particles can effectively retard the decomposition and merging of LAGBs, dislocation climbing and grain boundary sliding during subsequent thermo-mechanical treatment, thus enhancing the recrystallization temperature of the alloys [25]. Namely, the highly stable secondary Al_3(Sc, Zr) dispersoids that precipitated during the hot rolling and T6 heat treatment can strongly pin the dislocations and subgrain boundaries, thus causing substructure strengthening. The results are in agreement with other findings [19,22,27–30]. The efficacy of the dispersoids at inhibiting recrystallization can also be verified by the MAD maps shown in Figures 3 and 4, in which the accumulative fraction of the boundaries with misorientation angles > 15° are all lower than 12%.

Generally, the microstructure, texture and recrystallization kinetics are largely affected by the distribution of fine second-phase particles, and the existence of fine and densely distributed particles is conducive to pinning grain boundaries (Zener pinning) [19]. Figure 5b shows a high-resolution STEM image of the spherical particles, as indicated by the yellow solid and dotted arrows. The spherical precipitates with clear contrast are presented along the dislocations, HAGBs or subgrain boundaries and grain interior, which ultimately cause stabilization of the substructures by exerting a pinning force on the boundaries [27]. From the systematic research by Suresh et al. [19], the addition of the Sc element into the Al-Li alloy AA2195 resulted in the formation of densely distributed fine Al_3(Sc, Zr) dispersoids in the matrix. In addition, Al_3(Sc, Zr) dispersoids are coherent with the Al matrix [28]. Moreover, Duan et al. [29] also claimed that Al_3(Sc, Zr) precipitates have better drag ability to retard grain growth compared to other phases (Al_3Sc or Al_3Zr). According to Forbord et al. [30], the combined addition of Zr and Sc elements can resist recrystallization due to the formation of extremely fine, thermally stable Al_3(Sc, Zr) dispersoids, and the coarsening of these particles also dominates the recovery and recrystallization process. The XRD results (Figure 2d), SAED patterns and associated DF TEM micrographs (Figure 5d–g) also clearly confirmed the existence of the precipitates T_1 (Al_2CuLi), θ′ (Al_2Cu), δ′ (Al_3Li) and S′ (Al_2CuMg) with various morphologies in the studied sample, which are in accordance with previous reports on Al-Cu-Li alloys [31,32].

An increase in the rolling reduction leads to an improvement in the ultimate tensile strength and elongation of the peak-aged Sc-containing Al-Cu-Li alloy (Figure 6). Among the studied alloys, the Sc-containing alloy with a rolling reduction of 81.4% showed a better combination of ultimate tensile strength (480.4 MPa) and elongation (13.0%) relative to the other alloys. A slightly reduced ductility (12.97%) and a noticeable weakened tensile strength (459.6 MPa) are observed when the rolling reduction reached 88.2%. The strength of the Sc-containing Al-Cu-Li alloys is strongly linked to fine grains, precipitation, dispersion and substructure strengthening [33]. From the experimental results in Figures 3 and 4, it can be seen that a higher amount of rolling reduction results in finer grain size (Hall-Petch formula) in addition to retaining the morphology and distribution of the Al_3(Sc, Zr) dispersoids. The function of the Al_3(Sc, Zr) dispersoids is to promote the subgrain structures to be more steady, subsequently increasing the recrystallization temperature and enhancing the strength, which indicates that Sc has a prominent effect on the mechanical behaviors and recrystallization resistance. Previous studies [22] have suggested that both Al_3(Sc, Zr) dispersoid strengthening and substructure strengthening have contributed positively to strengthening the alloys. In the present study, microstructure analysis confirmed that a smaller grain size can be achieved in the alloys with a higher amount of rolling reduction (Figures 3 and 4), and the TEM images also exhibited the existence of substructures and Al_3(Sc, Zr) dispersoids in the studied alloys (Figure 5). Furthermore, given that the T_1 platelets with a high aspect ratio formed in the $\{111\}_{Al}$ plane have a close-packed (hcp) structure, they play a leading role in the strengthening effect of Al-Cu-Li alloys. The above

microstructure characteristics jointly contribute to the excellent mechanical behaviors of the studied samples.

5. Conclusions

Based on the obtained experimental results, the main conclusions are summarized as follows:

(1) With an increase in the rolling reduction, regardless of whether the T6 heat treatment was performed or not, the microstructure of the Sc-containing Al-Cu-Li alloy displays substructure characteristics. The volume fraction of the recrystallization of hot-rolled alloys is extremely low and basically remains unchanged, while the recrystallization volume fraction of the T6 treated alloys displays a rising trend on the whole, with values of 2.7%, 1.2%, 9.5% and 11.0%, respectively, as the rolling reduction increases.

(2) The precipitates of the Sc-containing Al-Cu-Li alloys are mainly numerous T_1 phases, orthogonal θ′ phases, fine dispersed δ′/β′ phases and a minute quantity of S′ phases. The fine, thermally stable Al_3(Sc, Zr) dispersoids that precipitated along the dislocations, subgrain boundaries or high-angle grain boundaries were responsible for the higher recrystallization resistance of the Sc-containing Al-Cu-Li alloys. Additionally, the precipitation of nano-sized Al_3(Sc, Zr) particles also remarkably impedes the growth of recrystallized grains during hot rolling and T6 heat treatment.

(3) Compared to the Sc-containing alloys with different rolling reductions, the alloy with a rolling reduction of 81.4% exhibited a better combination of tensile strength (480.4 MPa) and elongation (13.0%) due to grain refinement, precipitation, dispersion and substructure strengthening. As the rolling reduction increases, the strength of the alloys increases first and then decreases, while the elongation gradually increases and then enters a plateau, which is associated with the refined grains and the retention of the substructure characteristics.

Author Contributions: J.W.: Conceptualization, Investigation, Writing—original draft. Y.K.: Investigation, Methodology. W.X.: Writing—review and editing, Supervision. Y.L.: Project administration. D.Z.: Validation, Resources. S.L.: Software. All authors have read and agreed to the published version of the manuscript.

Funding: This work was supported by the Changzhou Sci&Tech Program (CJ20220061), Fundamental Research Funds for the Central Universities (B220203019) and the Postgraduate Research & Practice Innovation Program of Jiangsu Province (KYCX220673).

Institutional Review Board Statement: Not applicable.

Informed Consent Statement: Informed consent was obtained from all subjects involved in the study.

Data Availability Statement: Not applicable.

Conflicts of Interest: The authors declare no conflict of interest.

References

1. Wang, X.-M.; Li, G.-A.; Jiang, J.-T.; Shao, W.-Z.; Zhen, L. Influence of Mg content on ageing precipitation behavior of Al-Cu-Li-x alloys. *Mater. Sci. Eng. A* **2018**, *742*, 138–149. [CrossRef]
2. Liu, D.Y.; Wang, J.X.; Li, J.F.; Ma, Y.L.; Zhang, K.; Zhang, R.F. The effect of Ag element on the microstructure characteristic evolution of an Al-Cu-Li-Mg alloy. *J. Mater. Res. Technol.* **2020**, *9*, 11121–11134. [CrossRef]
3. Ma, Y.-L.; Li, J.-F.; Zhang, R.-Z.; Tang, J.-G.; Huang, C.; Li, H.-Y.; Zheng, Z.-Q. Strength and structure variation of 2195 Al-Li alloy caused by different deformation processes of hot extrusion and cold-rolling. Trans. *Nonferrous Met. Soc. China* **2020**, *30*, 835–849. [CrossRef]
4. Deschamps, A.; Garcia, M.; Chevy, J.; Davo, B.; De Geuser, F. Influence of Mg and Li content on the microstructure evolution of Al Cu Li alloys during long-term ageing. *Acta Mater.* **2017**, *122*, 32–46. [CrossRef]
5. Gumbmann, E.; Lefebvre, W.; De Geuser, F.; Sigli, C.; Deschamps, A. The effect of minor solute additions on the precipitation path of an Al Cu Li alloy. *Acta Mater.* **2016**, *115*, 104–114. [CrossRef]
6. Gumbmann, E.; De Geuser, F.; Sigli, C.; Deschamps, A. Influence of Mg, Ag and Zn minor solute additions on the precipitation kinetics and strengthening of an Al-Cu-Li alloy. *Acta Mater.* **2017**, *133*, 172–185. [CrossRef]

7. Li, B.; Pan, Q.L.; Yin, Z.M. Characterization of hot deformation behavior of as-homogenized Al-Cu-Li-Sc-Zr alloy using processing maps. *Mater. Sci. Eng. A* **2014**, *614*, 199–206. [CrossRef]
8. Xie, Y.; Deng, Y.; Wang, Y.; Guo, X. Effect of asymmetric rolling and subsequent ageing on the microstructure, texture and mechanical properties of the Al-Cu-Li alloy. *J. Alloys Compd.* **2020**, *836*, 155445. [CrossRef]
9. Liu, D.-Y.; Li, J.-F.; Liu, T.-L.; Ma, Y.-L.; Iwaoka, H.; Hirosawa, S.; Zhang, K.; Zhang, R.-F. Microstructure evolution and mechanical properties of Al-Cu-Li alloys with different rolling schedules and subsequent artificial ageing heat treatment. *Mater. Charact.* **2020**, *170*, 110676. [CrossRef]
10. Yang, X.; Huang, W.; Zhu, X.; Guo, F.; Hu, L.; Zhang, R. The effects of precipitates on microstructure and β-fiber texture in an Al-Cu-Li alloy during hot rolling. *Mater. Charact.* **2020**, *162*, 110186. [CrossRef]
11. Ye, F.; Mao, L.; Rong, J.; Zhang, B.; Wei, L.; Wen, S.; Jiao, H.; Wu, S. Influence of different rolling processes on microstructure and strength of the Al–Cu–Li alloy AA2195. *Prog. Nat. Sci.* **2022**, *32*, 87–95. [CrossRef]
12. Medjahed, A.; Moula, H.; Zegaoui, A.; Derradji, M.; Henniche, A.; Wu, R.; Hou, L.; Zhang, J.; Zhang, M. Influence of the rolling direction on the microstructure, mechanical, anisotropy and gamma rays shielding properties of an Al-Cu-Li-Mg-X alloy. *Mater. Sci. Eng. A* **2018**, *732*, 129–137. [CrossRef]
13. Kharakterova, M.L. Phase composition of aluminum-copper-scandium alloys at 450 and 500 °C. *Metally* **1991**, *4*, 191–194.
14. Kolobnev, N.I. Aluminum-Lithium Alloys with Scandium. *Met. Sci. Heat Treat.* **2002**, *44*, 297–299. [CrossRef]
15. Jia, M.; Zheng, Z.Q.; Gong, Z. Microstructure evolution of the 1469 Al-Cu-Li-Sc alloy during homogenization. *J. Alloys Compd.* **2014**, *614*, 131–139. [CrossRef]
16. Jia, M.; Zheng, Z.Q.; Luo, X.F. Influence of AlCuSc Ternary Phase on the Microstructure and Properties of 1469 Alloy. *Mater. Sci. Forum* **2014**, *794–796*, 1057–1062. [CrossRef]
17. Liu, D.-Y.; Wang, J.-X.; Li, J.-F. Microstructures evolution and mechanical properties disparity in 2070 Al-Li alloy with minor Sc addition. Trans. *Nonferrous Met. Soc. China* **2018**, *28*, 2151–2161. [CrossRef]
18. Huang, L.; Huang, J.; Liu, W.; Cao, L.; Li, S. Effect of minor Sc additions on precipitation and mechanical properties of a new Al-Cu-Li alloy under T8 temper. *J. Alloys Compd.* **2022**, *927*, 166860. [CrossRef]
19. Suresh, M.; Sharma, A.; More, A.; Nayan, N.; Suwas, S. Effect of Scandium addition on evolution of microstructure, texture and mechanical properties of thermo-mechanically processed Al-Li alloy AA2195. *J. Alloys Compd.* **2018**, *740*, 364–374. [CrossRef]
20. Zhang, H.F.; Zheng, Z.Q.; Lin, Y.; Xue, X.L.; Luo, X.F.; Zhong, J. Effects of small addition of Sc on microstructure and properties of 2099 Al-Li alloy. *J. Cent. South Univ. Sci. Technol.* **2014**, *45*, 1420–1427. (In Chinese)
21. Peng, Z.-W.; Li, J.-F.; Sang, F.-J.; Chen, Y.-L.; Zhang, X.-H.; Zheng, Z.-Q.; Pan, Q.-L. Structures and tensile properties of Sc-containing 1445 Al-Li alloy sheet. *J. Alloys Compd.* **2018**, *747*, 471–483. [CrossRef]
22. Ma, J.; Yan, D.; Rong, L.; Li, Y. Effect of Sc addition on microstructure and mechanical properties of 1460 alloy. *Prog. Nat. Sci.* **2014**, *24*, 13–18. [CrossRef]
23. Gao, Y.; Kuang, J.; Liu, G.; Sun, J. Effect of minor Sc and Fe co-addition on the microstructure and mechanical properties of Al-Cu alloys during homogenization treatment. *Mater. Sci. Eng. A* **2018**, *746*, 11–26. [CrossRef]
24. Dong, Y.; Ye, L.; Liu, X.; Ke, B.; Hu, T. Effects of large strain pre-deformation on creep age behavior and microstructural evolution of an Al-Cu-Li alloy. *Mater. Lett.* **2022**, *324*, 132699. [CrossRef]
25. Wang, Y.; Liu, H.; Ma, X.; Wu, R.; Sun, J.; Hou, L.; Zhang, J.; Li, X.; Zhang, M. Effects of Sc and Zr on microstructure and properties of 1420 aluminum alloy. *Mater. Charact.* **2019**, *154*, 241–247. [CrossRef]
26. Wang, Y.; Zhang, Z.; Wu, R.; Sun, J.; Jiao, Y.; Hou, L.; Zhang, J.; Li, X.; Zhang, M. Ambient-temperature mechanical properties of isochronally aged 1420-Sc-Zr aluminum alloy. *Mater. Sci. Eng. A* **2019**, *745*, 411–419. [CrossRef]
27. Hallem, H.; Lefebvre, W.; Forbord, B.; Danoix, F. Marthinsen. The formation of $Al_3(Sc_xZr_yHf_{1-x-y})$-dispersoids in aluminium alloys. *Mater. Sci. Eng. A* **2006**, *421*, 154–160. [CrossRef]
28. Deng, Y.; Yin, Z.; Zhao, K.; Duan, J.; He, Z. Effects of Sc and Zr microalloying additions on the microstructure and mechanical properties of new Al–Zn–Mg alloys. *J. Alloys Compd.* **2012**, *530*, 71–80. [CrossRef]
29. Duan, Y.L.; Xu, G.F.; Peng, X.Y.; Deng, Y.; Li, Z.; Yin, Z.M. Effect of Sc and Zr additions on grain stability and superplasticity of the simple thermal–mechanical processed Al–Zn–Mg alloy sheet. *Mater. Sci. Eng. A* **2015**, *648*, 80–91. [CrossRef]
30. Forbord, B.; Hallem, H.; Røyset, J.; Marthinsen, K. Thermal stability of $Al_3(Sc_x,Zr_{1-x})$- dispersoids in extruded aluminium alloys. *Mater. Sci. Eng. A* **2008**, *475*, 241–248. [CrossRef]
31. Khanikar, P.; Liu, Y.; Zikry, M. Experimental and computational investigation of the dynamic behavior of Al–Cu–Li alloys. *Mater. Sci. Eng. A* **2014**, *604*, 67–77. [CrossRef]
32. Zhang, S.F.; Zeng, W.D.; Yang, W.H.; Shi, C.L.; Wang, H.J. Ageing response of a Al-Cu-Li 2198 alloy. *Mater. Des.* **2014**, *63*, 368–374. [CrossRef]
33. Jiang, B.; Yi, D.; Yi, X.; Zheng, F.; Wang, H.; Wang, B.; Liu, H.; Hu, Z. Effect of trace amounts of added Sc on microstructure and mechanical properties of 2055 aluminum alloy. *Mater. Charact.* **2018**, *141*, 248–259. [CrossRef]